

Thermal evolution of Venus with argon degassing



Joseph G. O'Rourke^{a,*}, Jun Korenaga^b

^a Division of Geological and Planetary Sciences, California Institute of Technology, Pasadena, CA 91125, USA

^b Department of Geology and Geophysics, Yale University, New Haven, CT 06520, USA

ARTICLE INFO

Article history:

Received 17 February 2015

Revised 8 July 2015

Accepted 11 July 2015

Available online 17 July 2015

Keywords:

Venus, interior
Venus, atmosphere
Venus, surface
Thermal histories

ABSTRACT

Decades-old measurements of atmospheric and elemental surface composition constrain the history of Venus. In this study, we search for a model featuring continuous evolution in the stagnant-lid regime that predicts the present-day atmospheric mass of radiogenic argon and satisfies the other available constraints. For comparison, we also consider the end-member scenario of a single catastrophic resurfacing event. Thermal evolution simulations are performed that track the mass transport of argon and potassium and include a simple model of upwelling mantle plumes. Sensitivity analyses and linear regression are used to quantify the range of initial conditions that will produce desired values for key model output parameters. Decompression melting of passively upwelling mantle causes considerable mantle processing and crustal growth during the early evolution of Venus. Mantle plumes have negligible effects on recent crustal production, but may be important to local surface features. For a wide range of initial conditions, continuous evolution in the stagnant-lid regime predicts the correct amount of argon degassing, along with the absence of a global magnetic field, crustal and lithosphere thicknesses matching modern estimates, and volcanism consistent with the cratering record. Argon degassing does not uniquely constrain mantle dynamics, but the success of simple stagnant-lid models diminishes the need to invoke dramatic changes like catastrophic resurfacing.

© 2015 Elsevier Inc. All rights reserved.

1. Introduction

Venus, like Earth, is an engine that converts heat into interesting phenomena. Given their comparable orbital parameters, masses, and radii, Venus likely also differentiated into a silicate mantle and an iron-rich core, although its moment of inertia is not actually known (Bills et al., 1987). Dichotomous surface conditions are the most obvious proof that the evolution of Venus and Earth sharply diverged at some point. Earth is habitable and even clement, but greenhouse gases have raised surface temperatures on Venus to roughly 740 K (e.g., Bullock and Grinspoon, 2001). Whereas mantle dynamics cause frequent surface recycling on Earth through plate tectonics, mantle convection on Venus currently occurs below a rigid lithosphere that encompasses the entire planet (e.g., Kaula and Phillips, 1981; Solomatov and Moresi, 1996). In fact, all terrestrial planets in our Solar System besides Earth presently operate in this stagnant-lid regime of mantle convection (e.g., Schubert et al., 2001), which is perhaps natural because the viscosity of materials comprising terrestrial planets is strongly temperature-dependent (Solomatov, 1995). No consensus exists,

however, as to whether Venus exhibited dramatically different internal dynamics in the past, complicating the interpretation of surface geology.

Some models attempt to couple the evolution of both the interior and atmosphere of Venus (e.g., Phillips et al., 2001; Noack et al., 2012; Driscoll and Bercovici, 2013; Gillmann and Tackley, 2014). Greenhouse warming of the atmosphere may cause periodic increases in surface temperature to ~ 1000 K, possibly sufficient to cause episodic transitions from the stagnant- to mobile-lid regime by reducing the viscosity contrast across the lithosphere (Noack et al., 2012). High surface temperatures are also suggested to favor an episodic or stagnant-lid regime over plate tectonics for three reasons. First, a hot surface may eventually result in increasing mantle temperatures, causing convective stress to drop below the lithosphere yield stress on a ~ 1 Gyr timescale (Lenardic et al., 2008). Second, a non-Newtonian rheology based on damage theory predicts that high temperatures strengthen the lithosphere through a higher healing rate within ~ 100 Myr (Landuyt and Bercovici, 2009). Finally, high surface temperatures preclude the presence of surface water, which may be important to the generation of plate tectonics through lowering the brittle strength of lithosphere (e.g., Moresi and Solomatov, 1998; Korenaga, 2007).

Impact craters revealed by synthetic aperture radar images collected during NASA's Magellan mission provide major constraints

* Corresponding author.

E-mail address: jorourke@caltech.edu (J.G. O'Rourke).

on the evolution of Venus. The spatial coordinates of the ~ 1000 craters are indistinguishable from a random distribution. Only a few ($<10\%$) craters are obviously embayed by lava flows that breach their rims and cover their ejecta blankets. These two facts motivated the catastrophic resurfacing hypothesis, in which an episode of extreme volcanism lasting ~ 100 Myr covered the vast majority of the surface in km-thick flows (e.g., Schaber et al., 1992; Strom et al., 1994). According to studies of the likely impactor population and atmospheric screening, catastrophic resurfacing would have occurred between ~ 300 Ma and 1 Ga (e.g., McKinnon et al., 1997). Catastrophic resurfacing is also compatible with the so-called directional stratigraphy that categorizes morphologically similar terrains as globally synchronous units (e.g., Ivanov and Head, 2013). Theorists have invoked many mechanisms to explain catastrophic resurfacing, ranging from episodic subduction caused by lithosphere thickening above a warming mantle (Turcotte, 1993; Fowler and O'Brien, 1996) to brittle mobilization of the lithosphere (Moresi and Solomatov, 1998) to lid overturn caused by low yield stress (Armann and Tackley, 2012; Gillmann and Tackley, 2014). Transitions between the thick- and thin-lid branches of stagnant-lid convection (Reese et al., 1999) or a cessation of plate tectonics (e.g., Phillips and Hansen, 1998) have also been proposed. In any model, some recent volcanism is also required to explain the existence of young lava flows identified as high emissivity anomalies in Venus Express data (Smrekar et al., 2010) and sulfuric acid/water clouds, which would not persist without volcanic replenishment of SO_2 that is otherwise removed from the atmosphere within ~ 50 Myr (Fegley and Prinn, 1989; Bullock and Grinspoon, 2001).

Other evidence casts doubt on the idea of catastrophic resurfacing. Alternative stratigraphic studies suggest that local processes operating gradually throughout geologic time produced the surface features on Venus (Guest and Stofan, 1999). New mapping, for example, reveals that ribbon tesserae terrain records a geologic history that predates the formation of many other features attributed to catastrophic resurfacing (Hansen and Lopez, 2010). Non-catastrophic processes can also explain every characteristic of the cratering record. Localized resurfacing events can produce a random-looking distribution of craters and a low number of obviously embayed craters (Phillips et al., 1992; Bjonnes et al., 2012; O'Rourke et al., 2014). New studies argue that post-impact lava flows have partially filled the craters with radar-dark floors, which comprise $\sim 80\%$ of the total population (Wichman, 1999; Herrick and Sharpton, 2000; Herrick and Rumpf, 2011). Statistical modeling demonstrates that localized resurfacing events consisting of thin, morphologically indistinguishable flows can explain the number and spatial distribution of these dark-floored craters (O'Rourke et al., 2014). A minor amount of regionally concentrated volcanism can explain the relatively few, clustered craters that are obviously embayed in Magellan imagery.

Besides impact craters, the thicknesses of the crust and lithosphere of Venus provide important constraints on models of its history. Using gravity and topography data to construct a map of crustal thicknesses, however, requires an estimate of the mean crustal thickness, which is subject to large uncertainty. James et al. (2013) calculated the mean thickness of the crust as ~ 8 – 25 km, with an upper limit of ~ 45 km, using a two-layered crustal thickness inversion. Previous estimates of the present-day crustal thickness range from ~ 20 to 60 km (e.g., Smrekar, 1994; Simons et al., 1997; Nimmo and McKenzie, 1998). The observed topography may provide coarse upper bounds for crustal thickness because it would significantly relax if the crust were thick enough to cause lateral flow (Nimmo and Stevenson, 2001) or to undergo the phase transition from (metamorphosed) basalt to eclogite (e.g., Namiki and Solomon, 1993). Constraints on the thickness of the mantle lithosphere of Venus are likewise loose. Some authors

favor a relatively thick lithosphere, usually ~ 200 – 400 km (e.g., Turcotte, 1993; Solomatov and Moresi, 1996), but data permit values as high as ~ 600 km (Orth and Solomatov, 2011). Thinner (~ 100 km) lithosphere allows a larger magnitude of melt generation to explain recent resurfacing (e.g., Schubert, 1994; Smrekar, 1994; Simons et al., 1997; Nimmo and McKenzie, 1998).

Observations suggest that the core of Venus is likely cooling, but not convecting with sufficient vigor to produce a dynamo. Features in gravity field and topography data that are associated with large volcanic rises, high radar emissivity anomalies, and stratigraphically young flows indicate the presence of several plumes upwelling from the lower mantle (Stofan et al., 1995; Smrekar et al., 2010; Smrekar and Sotin, 2012). The existence of plumes might imply, at minimum, a positive heat flux across the core/mantle boundary (e.g., Weizman et al., 2001). However, Venus today has no global magnetic field (Phillips and Russell, 1987). Paleomagnetic evidence indicates that Earth's dynamo, in contrast, has persisted for more than 3.4 Gyr (Tarduno et al., 2010). Perhaps Venus lacks an inner core and thus compositional convection or, less likely, the core is completely frozen solid (Stevenson et al., 1983; Stevenson, 2003). Stagnant-lid convection is inefficient compared to plate tectonics, so the mantle will tend to insulate the core and limit cooling (e.g., Driscoll and Bercovici, 2014). Recent theoretical and experimental work indicates that the thermal conductivity of iron alloys at core conditions is possibly very high, meaning that driving a dynamo with thermal convection alone is quite difficult (e.g., Pozzo et al., 2012; Gomi et al., 2013). Significant cooling still is required even if conventionally low values for thermal conductivity are actually correct (e.g., Zhang et al., 2015). Another possibility is that the core became compositionally stratified and thus convectively stable during accretion, since more light elements tend to enter core material as pressure/temperature conditions increase (e.g., Rubie et al., 2015).

Degassing of noble-gas elements has long been incorporated into thermal evolution models for Earth (e.g., Sleep, 1979; Tajika and Matsui, 1993), but few studies have applied the same techniques to Venus. Argon-40, in particular, is produced by the decay of radioactive ^{40}K in the interior of Venus and released to the atmosphere through volcanism. The present-day atmospheric abundance of ^{40}Ar has been measured as 3.3 ± 1.1 ppb relative to the mass of Venus or $1.61 \pm 0.54 \times 10^{16}$ kg (von Zahn et al., 1983). This datum has been used to test the plausibility of ad hoc crustal production histories for Venus (Namiki and Solomon, 1998) and to place more general constraints on crustal thickness and the evolution of Venus (Kaula, 1999). A 2D cylindrical model with strongly temperature- and pressure-dependent viscosity confirmed that a substantial fraction of argon could degas even without plate tectonics (Xie and Tackley, 2004). Different modes of mantle convection may cause varying amounts of volcanism and thus degassing (e.g., O'Neill et al., 2014). One experimental study potentially diminishes the utility of ^{40}Ar degassing as a constraint on planetary evolution, however, claiming that argon may be more compatible with basaltic melts than olivine and that argon diffusion takes place very slowly (Watson et al., 2007). But a more recent investigation with a different experimental approach suggests that the results of Watson et al. (2007) may not properly represent bulk crystalline properties, thus supporting the usual assumptions that argon is incompatible and that diffusion can occur quickly at high temperatures (Cassata et al., 2011).

The purpose of this study is to evaluate whether models of the evolution of Venus can predict the present-day atmospheric mass of radiogenic argon while satisfying other available constraints. We use parameterized models of stagnant-lid convection, which have long been applied to the terrestrial planets in our Solar System (e.g., Stevenson et al., 1983). A scaling law of stagnant-lid

convection that takes into account complications from mantle processing and crustal formation, however, was only developed recently (Korenaga, 2009). This formulation has been applied to Mars (Fraeman and Korenaga, 2010) and, with modification, to massive terrestrial planets (O'Rourke and Korenaga, 2012). Our new contribution in this study is the self-consistent incorporation of models for both argon degassing and mantle plumes.

2. Quantifying argon degassing

In this section, we discuss the fundamental assumptions underlying models of argon degassing during the thermochemical evolution of Venus. The initial abundances of ^{40}Ar in the atmosphere and interior are usually considered negligible (e.g., Namiki and Solomon, 1998; Kaula, 1999). Thus, radioactive decay of ^{40}K produced all of the ^{40}Ar that is observed today. For a closed system, we can calculate the abundance of ^{40}Ar as a function of time:

$$[^{40}\text{Ar}(t)] = \frac{\lambda_{\text{Ar}}}{\lambda_{\text{tot}}} [^{40}\text{K}(0)](1 - e^{-\lambda_{\text{tot}}t}), \quad (1)$$

where $\lambda_{\text{tot}} = \lambda_{\text{Ar}} + \lambda_{\text{Ca}}$ is the decay constant for ^{40}K , with $\lambda_{\text{Ar}} = 0.0581 \text{ Gyr}^{-1}$ and $\lambda_{\text{Ca}} = 0.4962 \text{ Gyr}^{-1}$ (Kaula, 1999). The abundance of ^{40}K obeys:

$$[^{40}\text{K}(t_p)] = [^{40}\text{K}(0)]e^{-\lambda_{\text{tot}}t_p}, \quad (2)$$

where $t_p = 4.5 \text{ Gyr}$ has elapsed since accretion. We assume $^{40}\text{K}/\text{K} = 1.165 \times 10^{-4}$ (Kaula, 1999).

The present-day abundances of radioactive isotopes on both Venus and Earth are only loosely constrained. Data from four Venera and Vega lander sites on Venus indicate $\text{K}/\text{U} = 7220 \pm 1220$ (Kaula, 1999). Elemental abundances were measured with very poor precision on Venus relative to available data from Earth and Mars. Furthermore, these landers only visited the lowland volcanic plains, which themselves exhibit chemical heterogeneity, leaving many geologic terrains on Venus unexplored (Treiman, 2007). In any case, estimated values of Earth's K/U are much higher, e.g., $\text{K}/\text{U} = 13,800 \pm 1300$ in Arevalo et al. (2009). We might expect a relatively low K/U for Venus because potassium is volatile and Venus is closer to the Sun than Earth, but simulations of planetary formation and migration suggest that Venus and Earth might have accreted with similar inventories of volatile elements (e.g., Rubie et al., 2015). So, they may actually have similar K/U . Kaula (1999) assumed that $[\text{U}] = 21 \text{ ppb}$ for Venus, corresponding to the conventional geochemical model of Earth (e.g., McDonough and Sun, 1995). However, even for Earth, this value has nontrivial uncertainty. A plausible lower bound for Earth's mantle is $[\text{U}] = 13 \text{ ppb}$ (Lyubetskaya and Korenaga, 2007). Kaula (1999) calculated that $24 \pm 10\%$ of the available ^{40}Ar resides in the atmosphere if $\text{K}/\text{U} = 7220$ and $[\text{U}] = 21 \text{ ppb}$. As shown in Fig. 1, however, Venus may have degassed as much as $\sim 50\%$ if $[\text{U}] = 13 \text{ ppb}$. Alternatively, if $[\text{U}] = 24 \text{ ppb}$ and $\text{K}/\text{U} = 15,200$, which are near the upper limits of plausible values for Earth, then Venus may be only $\sim 10\%$ degassed.

Despite these uncertainties, we can model the effects of crustal production and degassing on the planetary budget of K , ^{40}K , and ^{40}Ar . Argon-40 partitioning is assumed to follow the usual formula for accumulated fractional melting (Shaw, 1970):

$$\frac{[^{40}\text{Ar}]_c}{[^{40}\text{Ar}]_{\text{SM}}} = \frac{1}{\phi} \left[1 - (1 - \phi)^{1/D} \right], \quad (3)$$

where $[^{40}\text{Ar}]_c$ and $[^{40}\text{Ar}]_{\text{SM}}$ are the abundances of ^{40}Ar in the newly generated crust and the source mantle, respectively. The melt fraction is ϕ and the bulk distribution coefficient is D . Because D is very small, we approximate $(1 - \phi)^{1/D} \approx 0$ (e.g., Kaula, 1999). Likewise,

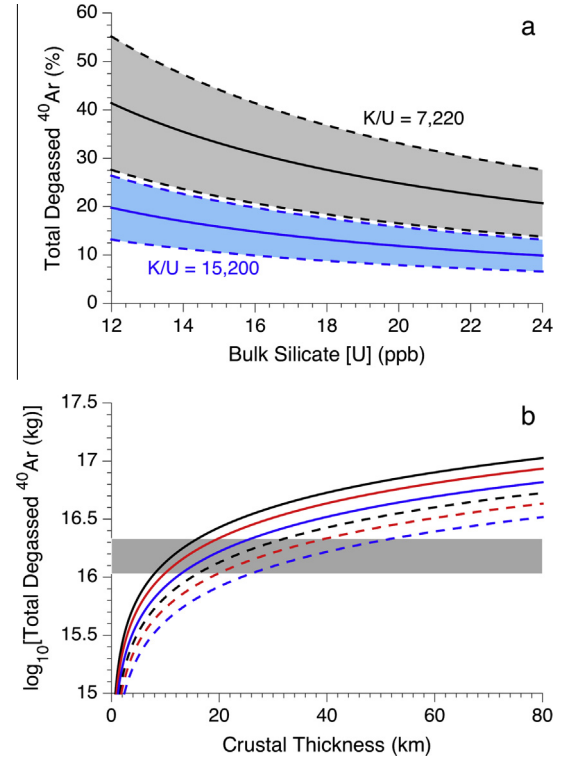


Fig. 1. (a) Percentage of the total amount of ^{40}Ar that has been degassed from the interior to the atmosphere of Venus as a function of the bulk silicate [U] at present. Black and blue lines represent calculations assuming $\text{K}/\text{U} = 7220$ and $15,200$, respectively. Shaded regions are $1-\sigma$ uncertainty envelopes derived from the formal error on the measurement of the present-day amount of atmospheric ^{40}Ar . (b) Predictions of the present-day atmospheric mass of radiogenic ^{40}Ar as a function of crustal thickness produced in a single event with $\phi = 0.025$ and 0.05 (solid and dashed lines, respectively) and $[\text{U}(t_p)] = 21, 17,$ and 13 ppb (black, red, and blue lines, respectively). The measured value ($1-\sigma$ range) is shaded in gray (von Zahn et al., 1983). (For interpretation of the references to color in this figure legend, the reader is referred to the web version of this article.)

we assume $[\text{K}]_c/[\text{K}]_{\text{SM}} \approx [^{40}\text{K}]_c/[^{40}\text{K}]_{\text{SM}} \approx 1/\phi$. For a given crustal thickness h_c , the associated crustal volume V_c can be calculated with a geometrical relation (Fraeman and Korenaga, 2010):

$$V_c = \frac{4\pi}{3} [R_p^3 - (R_p - h_c)^3], \quad (4)$$

where R_p is the radius of Venus. The volume of mantle processed to make crust is simply $V_{\text{proc}} = V_c/\phi$.

Two additional assumptions allow us to calculate the amount of ^{40}Ar degassed as a result of an episode of crustal production. First, if all ^{40}Ar from the processed mantle is degassed, then we can calculate the mass of ^{40}Ar immediately added to the atmosphere:

$$M_i = [^{40}\text{Ar}(t_c)]_{\text{SM}} \left(\frac{\rho_m V_c}{\phi} \right), \quad (5)$$

where t_c is the time of crustal production and ρ_m is the density of the mantle. Next, we assume that argon diffusion through the crust is effectively instantaneous. This is reasonable because high surface temperatures on Venus should allow argon to escape feldspar and olivine grains within $\sim 1 \text{ Myr}$ and then travel quickly through grain boundaries to the surface (Namiki and Solomon, 1998; Kaula, 1999). The mass of ^{40}Ar generated by radioactive decay in the crust and then released by diffusion until the present is therefore:

$$M_d = \rho_m V_c [^{40}\text{K}(t_c)]_c \left(\frac{\lambda_{\text{Ar}}}{\lambda_{\text{tot}}} \right) [1 - e^{-\lambda_{\text{tot}}(t_p - t_c)}]. \quad (6)$$

The total mass of atmospheric ^{40}Ar expected at present is simply $M_{atm,^{40}\text{Ar}} = M_i + M_d$. Atmospheric escape of argon, unlike radiogenic helium, is assumed to be negligible. As a simple problem, we calculate the unrealistic, end-member example of a single episode of crustal formation from partial melting of the primitive mantle (PM). In this case,

$$M_{atm,^{40}\text{Ar}} = [^{40}\text{K}(0)]_{PM} \left(\frac{\rho_m V_c}{\phi} \right) \left(\frac{\lambda_{\text{Ar}}}{\lambda_{\text{tot}}} \right) (1 - e^{-\lambda_{\text{tot}} t_p}), \quad (7)$$

which is independent of t_c . Fig. 1 illustrates that the production of ~10–50 km of crust in a single event could explain the observed atmospheric mass of radiogenic argon for plausible values of ϕ and $[U(t_p)]$. However, realistic models must consider how crustal production occurs throughout geologic time.

3. Theoretical formulation

The thermal and chemical evolution of Venus may be simulated with a one-dimensional parameterized model using scaling laws built on numerical models (Korenaga, 2009). Assuming that Venus is initially differentiated into the primitive mantle and the core, we use the thermal and chemical structure shown in Fig. 2. The stagnant lid is a thermal boundary layer consisting of the mantle lithosphere (ML) and the chemically distinct crust. The depleted mantle lithosphere (DML) is the upper region of the primitive mantle (PM) that has been processed by partial melting to form crust, which is always thinner than the ML. The convecting mantle that underlies the stagnant lid becomes more depleted than the PM over time, as the DML could delaminate if cooled enough to overcome its chemical buoyancy and become mixed with the convecting mantle. The convecting mantle is thus referred to as the source mantle (SM). The evolution of these layers is simulated using the formulation from O'Rourke and Korenaga (2012) with some modifications to track mantle plumes and mass transport of argon and potassium. To be self-contained, the entire procedure is briefly summarized below.

3.1. Model description

The two governing equations are the energy balances for the core and the mantle. For the core:

$$\left[4\pi R_i^2 \rho_c (L_c + E_g) \frac{dR_i}{dT_{cm}} - \frac{4}{3} \pi R_c^3 \eta_c \rho_c C_c \right] \frac{dT_{cm}}{dt} = 4\pi R_c^2 F_c, \quad (8)$$

where R_i and R_c are the radii of the inner and entire core, respectively; E_g is the gravitational energy liberated per unit mass of the inner core; L_c is the latent heat of solidification associated with the inner core; T_{cm} is the temperature at the core/mantle boundary; η_c is the ratio of T_{cm} , the temperature at the core side of the core/mantle boundary, to the average core temperature; C_c is the specific heat of the core; ρ_c is the density of the core; and F_c is the heat flux out of the core. We use the method of Stevenson et al. (1983) to parametrize core cooling, including the calculation of F_c , which assumes that the liquid outer core is chemically homogenous. We calculate the liquidus with the concentration of light elements in the core fixed to 0.1 by analogy to Earth. However, we use the viscosity given below by Eq. (11) to calculate the thickness of the lower boundary layer in the mantle. Stevenson et al. (1983) used a much lower viscosity, which yields a thin boundary layer and a very small (<15 K) core/mantle temperature contrast. For the mantle (Hauck and Phillips, 2002):

$$\frac{4}{3} \pi (R_m^3 - R_c^3) \left(H_m - \eta_m \rho_m C_m \frac{dT_u}{dt} \right) - \rho_m f_m L_m = 4\pi (R_m^2 F_m - R_c^2 F_c), \quad (9)$$

where R_m is the radius of the mantle; H_m is the volumetric heat production of the mantle; η_m is the ratio of the average temperature of the mantle to T_u , the potential temperature of the mantle; ρ_m is the density of the mantle; C_m is the specific heat of the mantle; f_m is volumetric melt production (explained below) with associated latent heat release, L_m ; and F_m is the heat flux across the mantle/crust boundary.

We consider heat production from the radioactive decay of ^{40}K , ^{235}U , ^{238}U , and ^{232}Th . Volumetric radiogenic heating may be calculated (Korenaga, 2006):

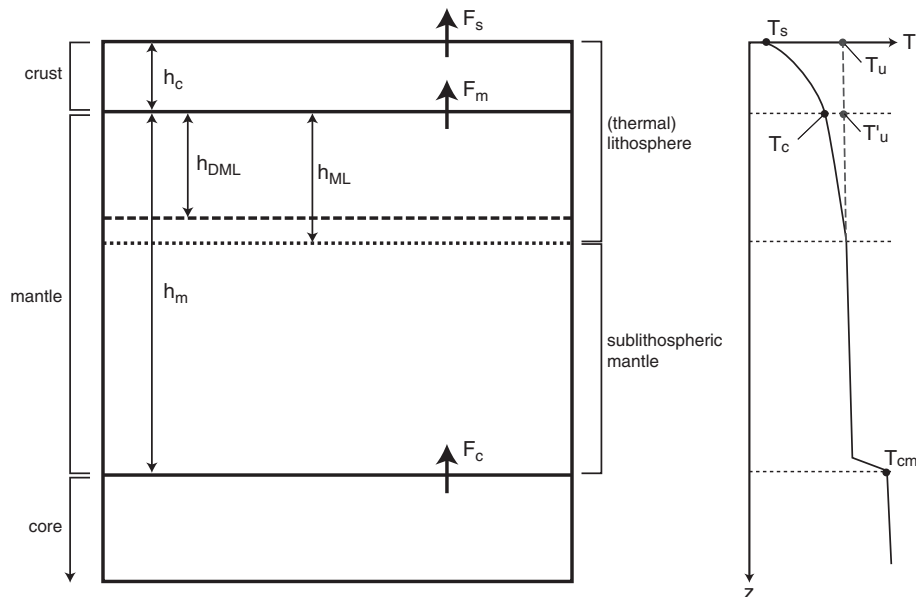


Fig. 2. Cartoon showing the assumed thermal (right) and chemical (left) structure of Venus, reproduced from Fraeman and Korenaga (2010) and O'Rourke and Korenaga (2012). Key model parameters are illustrated.

$$H_m(t) = \rho_m \sum_n c_{n,0} P_n(0) e^{-\lambda_n t}, \quad (10)$$

where for each isotope, $c_{n,0}$ is the initial abundance, $P_n(0)$ is the initial specific heat production, and λ_n is the decay constant. Constants used to calculate radiogenic heat production are taken from [Kaula \(1999\)](#) and [Korenaga \(2006\)](#). Initial isotopic abundances are calculated from the present-day [U]_{PM} and K/U, assuming that the following ratios are valid at the present for the primitive mantle ([Korenaga, 2006](#)): $^{40}\text{K}/\text{K} = 1.165 \times 10^{-4}$, $^{238}\text{U}/\text{U} = 0.9927$, $^{235}\text{U}/\text{U} = 0.0072$, and $^{232}\text{Th}/\text{U} = 4$.

Mantle viscosity is parametrized assuming a Newtonian rheology ([Fraeman and Korenaga, 2010](#)):

$$\eta(T_u, C_{SM}^W) = A \exp \left[\frac{E}{RT_u} + (1 - C_{SM}^W) \log \Delta\eta_w \right], \quad (11)$$

where R is the universal gas constant, A is a preexponential constant calculated assuming a reference viscosity η_0 at a temperature $T_u^* = 1573$ K, and E is the activation energy. We use values of E appropriate to the rheology of the upper mantle, such as ~ 300 kJ mol $^{-1}$ for dry olivine ([Karato and Wu, 1993](#)). Near the core/mantle boundary, E may increase to ~ 520 kJ mol $^{-1}$, but absolute temperature rises as well ([Yamazaki and Karato, 2001](#)). Melting may cause dehydration of the mantle over time. We parametrize the resulting increase in viscosity using $\Delta\eta_w$, the viscosity contrast between dry and wet mantle, and C_{SM}^W , the normalized water concentration within the mantle, which has an initial value of one and decreases towards zero ([Fraeman and Korenaga, 2010](#); [O'Rourke and Korenaga, 2012](#)).

With the above viscosity formulation, two non-dimensional parameters characterize thermal convection in the stagnant-lid regime ([Solomatov, 1995](#)). First, the internal Rayleigh number quantifies potential convective vigor ([Fraeman and Korenaga, 2010](#)):

$$Ra_i = \frac{\alpha \rho_m g (T_u' - T_c) h_m^3}{\kappa \eta (T_u, C_{SM}^W)}, \quad (12)$$

where α is the coefficient of thermal expansion; T_u' and T_c are the mantle potential temperature defined at the top of the mantle and the temperature at the bottom of the crust (called the ‘‘Moho’’ temperature), respectively; h_m is the thickness of the mantle; and κ is thermal diffusivity. Second, we use the Frank-Kamenetskii parameter ([Solomatov, 1995](#); [Fraeman and Korenaga, 2010](#)):

$$\theta = \frac{E(T_u' - T_c)}{RT_u^2}. \quad (13)$$

With these two parameters, we calculate the average convective velocity of passive upwellings beneath the stagnant lid ([Solomatov and Moresi, 2000](#)):

$$u = 0.38 \frac{\kappa}{h_m} \left(\frac{Ra_i}{\theta} \right)^{1/2}. \quad (14)$$

The Nusselt number is a non-dimensional measure of convective heat flux. A simple scaling exists for stagnant-lid convection with purely temperature-dependent viscosity ([Solomatov and Moresi, 2000](#)), but including the effects of dehydration stiffening and compositional buoyancy requires the Nusselt number to be calculated with the local stability analysis at each time step, which precludes an analytic expression. The symbolic functionality is ([Korenaga, 2009](#)):

$$Nu = f(Ra, E, T_u, T_c, h_{DML}, h_m, \Delta\eta_m, \Delta\rho), \quad (15)$$

where h_{DML} is the thickness of the depleted mantle lithosphere and $\Delta\eta_m$ and $\Delta\rho$ respectively represent the viscosity and density

contrasts between the depleted mantle and the source mantle. Finally, the thickness of the thermal boundary layer in the mantle, termed the mantle lithosphere, is calculated ([Fraeman and Korenaga, 2010](#)):

$$h_{ML} = \frac{h_m}{Nu}. \quad (16)$$

During stagnant-lid convection, passively upwelling mantle rock partially melts as its pressure decreases. As in [Fraeman and Korenaga \(2010\)](#) and [O'Rourke and Korenaga \(2012\)](#), we calculate the initial pressure of melting ([Korenaga, 2002](#)):

$$P_i = \frac{T_u - 1423}{1.20 \times 10^{-7} - (dT/dP)_s}, \quad (17)$$

where $(dT/dP)_s$ is the adiabatic mantle gradient, assuming that the Venusian mantle follows the solidus of dry peridotite. Melting stops at the base of the mantle lithosphere, with the final pressure of melting calculated as:

$$P_f = \rho_m g (h_c + h_{ML}), \quad (18)$$

where we assume for simplicity that ρ_m is the density of the lithosphere. As long as $P_i > P_f$, there is a melting zone with thickness d_m and average melt fraction equal to

$$\phi = \frac{P_i - P_f}{2} \left(\frac{d\phi}{dP} \right)_s, \quad (19)$$

where $(d\phi/dP)_s$ is the melt productivity by adiabatic decompression. Finally, we calculate the volumetric melt production from pressure release melting ([Fraeman and Korenaga, 2010](#)):

$$f_m = \frac{2d_m u \phi}{h_m} 4\pi R_c^2, \quad (20)$$

where u is calculated in Eq. (14) and the numerical coefficients arise from the assumption that the passively upwelling mantle is cylindrical.

3.2. Upwelling mantle plumes

Upwelling plumes from the core/mantle boundary may transport heat to the top of the mantle if there exists a thermal boundary layer at the bottom of the mantle. [Smrekar and Sotin \(2012\)](#) argued that the temperature difference, ΔT_{cm} , must exceed the viscous temperature scale, $\Delta T_\eta = |1/(\partial \ln \eta / \partial T)|$, to produce plumes with realistically large buoyancy fluxes. From Eq. (11), $\Delta T_\eta = RT_u^2/E \sim 80$ K for $T_u = 1700$ K and $E = 300$ kJ mol $^{-1}$. However, we assume that plumes can transport some heat flux as long as $\Delta T_{cm} > 0$. The maximum volume of material available to form plumes is $V_p = 4\pi R_c^2 \delta_c$, where δ_c is the thickness of the thermal boundary layer on the mantle side of the core/mantle boundary and R_c is the radius of the core. Material in the thermal boundary layer is replenished on time scale $\tau = \delta_c^2/\kappa$, where κ is thermal diffusivity. The maximum volume of plume material that can be delivered to the lithosphere in time Δt is therefore ([Weizman et al., 2001](#)):

$$S_{p,max} = \Delta t \left(\frac{V_p}{\tau} \right) = \Delta t \left(\frac{4\pi R_c^2 \kappa}{\delta_c} \right). \quad (21)$$

Since plumes likely cannot traverse the entire mantle in one time step, the real volumetric flux should be less than this maximal estimate. Likewise, only a fraction of the boundary layer will actually form plumes. The rate of heat delivery by plumes may thus be expressed as ([Weizman et al., 2001](#)):

$$F_p = S_p \left(\frac{\rho_m C_m \Delta T_p}{4\pi(R_p - h_c)^2} \right), \quad (22)$$

where ΔT_p is the plume temperature anomaly, which we assume is equal to ΔT_{cm} , the total temperature difference across the core/mantle boundary, and R_p is the radius of Venus. Assuming that $R_p \gg h_c$, we may use Eqs. (21) and (22) to write an equation for the maximum heat flux from mantle plumes:

$$F_{p,max} = \frac{k\Delta T_{cm}}{\delta_c} \left(\frac{R_c}{R_p} \right)^2 = F_c \left(\frac{R_c}{R_p} \right)^2. \quad (23)$$

Hence, as expected, the heat flux from mantle plumes does not exceed the heat flux from the core/mantle boundary. We assume that the heat flux from plume upwelling is some fraction of the core heat flux, i.e., $F_p = f(R_c/R_p)^2 F_c$, where $0 \leq f < 1$. Thus, we may calculate:

$$S_p = fF_c \left(\frac{R_c}{R_p} \right)^2 \left[\frac{4\pi(R_p - h_c)^2}{\rho_m C_m \Delta T_p} \right]. \quad (24)$$

We suppress magmatism from these mantle plumes (but not from passively upwelling mantle) for the first 0.5 Gyr of each simulation to avoid unrealistically large values from the “hot start” of the core. Choosing $f \leq 0.5$ compensates for the likely overestimation of ΔT_p in this formulation and the decrease in excess temperature that occurs as plumes rise though the mantle (Leng and Zhong, 2008).

Internal heating and surface cooling drive mantle convection in the absence of mantle plumes. In this case, the mantle heat flux is the heat conducted through the upper thermal boundary layer (Fraeman and Korenaga, 2010):

$$F'_m = k \frac{Nu(T'_u - T_c)}{h_m} \quad (25)$$

Mantle plumes provide an additional heat flux at the base of the upper boundary layer. We assume that plumes do not affect its overall structure since the heat flux from mantle plumes is relatively small. Thus, the total mantle heat flux is calculated as $F_m = F'_m + F_p$ (Weizman et al., 2001).

We assume that the upwelling plume reaches the base of the lithosphere within the time step of duration Δt and undergoes partial melting. The initial pressure of plume melting, $P_{i,p}$, is calculated using Eq. (17) with the substitution of $T_{u,p} = T_u + \Delta T_{cm}$, which is the potential temperature of the mantle plumes, i.e., the temperature that they would have if raised from the core/mantle boundary to the surface along an adiabatic temperature gradient. The final pressure of melting and the average melt fraction in the melting region are calculated using Eqs. (18) and (19). Finally, the total melt productivity of the mantle plumes is simply $f_p = \phi_p S_p$, assuming that the entire plume passes through the region of melting.

3.3. Mass transport of argon and potassium

We model argon degassing and the mass transport of potassium using a variation of the method that Fraeman and Korenaga (2010) used to track the dehydration of the mantle. The amount of mantle that has been melted during a time interval Δt is (Fraeman and Korenaga, 2010):

$$\Delta V_{proc} = \Delta t \left(\frac{f_m}{\phi} + S_p \right). \quad (26)$$

The associated increase in crustal volume is $\Delta V_c = (f_m + f_p)\Delta t$. By mass balance, ignoring small density differences, the change in the volume of the DML is $\Delta V_{DML} = \Delta V_{proc} - \Delta V_c$. Assuming that $^{40}\text{K}/\text{K}$ is negligibly small, the mass of potassium in the PM is calculated as

$$M_{PM,K} = \rho_m V_{PM} [\text{K}(0)]_{PM}, \quad (27)$$

where the volume of the PM, V_{PM} , is constant. The volume of the convecting SM is simply $V_{SM}(t) = V_{PM} - V_{DML}(t) - V_c(t)$. So, the crustal mass of potassium may be tracked as

$$M_{c,K}(t) = M_{c,K}(t - \Delta t) + \rho_m \Delta V_{proc} [\text{K}(t)]_{SM}, \quad (28)$$

where the abundance of potassium in the convecting SM, $[\text{K}(t)]_{SM}$, is calculated as

$$[\text{K}(t)]_{SM} = \frac{M_{PM,K} - M_{c,K}(t)}{\rho_m V_{SM}(t)}. \quad (29)$$

Finally, the crustal abundances of K and ^{40}K are their crustal masses divided by $\rho_c V_c(t)$, where we assume that $\rho_c \approx \rho_m$ for simplicity.

Tracking the transport of ^{40}K is more complicated because of radioactive decay. The mass in the PM decreases with time as

$$M_{PM,^{40}\text{K}}(t) = \rho_m V_{PM} [^{40}\text{K}(0)]_{PM} e^{-\lambda_{tot} t}. \quad (30)$$

The crustal mass of ^{40}K is thus calculated as

$$M_{c,^{40}\text{K}}(t) = M_{c,^{40}\text{K}}(t - \Delta t) e^{-\lambda_{tot} \Delta t} + \rho_m \Delta V_{proc} [^{40}\text{K}(t)]_{SM}, \quad (31)$$

where the abundance of ^{40}K in the SM is simply

$$[^{40}\text{K}(t)]_{SM} = \frac{M_{PM,^{40}\text{K}}(t) - M_{c,^{40}\text{K}}(t)}{\rho_m V_{SM}(t)}. \quad (32)$$

We assume that all ^{40}Ar partitioned into or generated within the crust is instantaneously released to the atmosphere. Thus, we can track the atmospheric mass of ^{40}Ar

$$M_{atm,^{40}\text{Ar}}(t) = M_{atm,^{40}\text{Ar}}(t - \Delta t) + \rho_m \Delta V_{proc} [^{40}\text{Ar}(t)]_{SM} + \rho_c V_c(t) [^{40}\text{K}(t)]_c \left(\frac{\lambda_{tot}}{\lambda_{Ar}} \right) (1 - e^{-\lambda_{tot} \Delta t}). \quad (33)$$

The mass of ^{40}Ar in the PM and its abundance in the SM, respectively, are calculated as

$$M_{PM,^{40}\text{Ar}}(t) = M_{PM,^{40}\text{K}} \left(\frac{\lambda_{tot}}{\lambda_{Ar}} \right) (1 - e^{-\lambda_{tot} t}) \quad (34)$$

and

$$[^{40}\text{Ar}(t)]_{SM} = \frac{M_{PM,^{40}\text{Ar}}(t) - M_{atm,^{40}\text{Ar}}(t)}{\rho_m V_{SM}(t)}. \quad (35)$$

Incorporating incomplete partitioning of argon or slow diffusion would require more complicated equations. Eqs. (33) and (35) would only give upper and lower limits for $M_{atm,^{40}\text{Ar}}(t)$ and $[\text{Ar}(t)]_{SM}$, respectively. Additionally, if crustal recycling occurs faster than argon diffusion, then less degassing would be expected for a given amount of mantle processing.

4. Numerical models

The parametrized model described above was used to calculate the thermal and chemical evolution of Venus in the stagnant-lid regime. All permutations of the following sets of parameters and initial conditions were used: activation energy, $E = 300, 350,$ and 400 kJ mol^{-1} ; present-day K/U = 7220, 10,510, and 13,800; present-day uranium abundance, $[U(t_p)]_{PM} = 13, 15, 17, 19,$ and 21 ppb ; initial mantle potential temperature, $T_u(0) = 1500, 1600, 1700, 1800,$ and 1900 K ; initial core/mantle boundary temperature, $T_{cm}(0) = 4000, 4200,$ and 4400 K ; and reference viscosity, $\log_{10}(\eta_0) = 19, 19.5, 20$ and 20.5 . The parameter governing how the progressive dehydration of the mantle increases its viscosity is set to $\Delta \eta_w = 100$. We also assumed that compositional buoyancy of the DML, $d\rho/d\phi = 120 \text{ kg m}^{-3}$, which controls $\Delta\rho$ in Eq. (15) (Fraeman and Korenaga, 2010; O'Rourke and Korenaga, 2012).

Values for fixed constants and definitions of other key parameters are listed in Table 1. The simulations were numerically integrated with the Euler method for 4.5 Gyr with a time step of 1 Myr.

The parameterization of mantle plume upwelling may affect the calculated history of crustal production and argon degassing. We set $f = 0.25$ for most simulations. But we also performed a sensitivity analysis with another 50 simulations to test the importance of the large uncertainty in this parameter. Fixing $E = 300 \text{ kJ mol}^{-1}$, $K/U = 7220$, $[U(t_p)]_{PM} = 17 \text{ ppb}$, $T_u(0) = 1900 \text{ K}$, $T_{cm}(0) = 4200 \text{ K}$, and $\log_{10}(\eta_0) = 20.5$, we varied f within the plausible range of 0.01–0.5 in increments of 0.01. For each simulation, we focus on $M_{atm,^{40}\text{Ar}}(t_p)$, $h_c(t_p)$, and $\Delta h_{c,0.5}$, the thickness of crust produced in the last 0.5 Gyr.

Limited constraints were placed on the simulation results. In particular, we only accepted simulations with realistic crustal thicknesses, i.e., $1 \text{ km} \leq h_c(t_p) \leq 75 \text{ km}$. Out of 2700 total, 1284 failed this criterion because they featured extremely high or low values of K/U , $[U(t_p)]_{PM}$, $T_u(0)$, and/or $T_{cm}(0)$. With $K/U = 7220$, present-day $[U]_{PM} = 21$ and 13 ppb are equivalent to initially 7.07×10^{-8} and $4.38 \times 10^{-8} \text{ W m}^{-3}$ of volumetric radiogenic heating, respectively. Important model outputs included time series

Table 1

List of key model parameters. References: [1] Stevenson et al. (1983), [2] Korenaga (2006), [3] Noack et al. (2012), [4] Spohn (1991), [5] Fraeman and Korenaga (2010), and [6] Korenaga (2002). Variables are chosen or calculated as described in the text.

Parameter	Definition	Value	Units	Ref.
<i>Constant</i>				
k	Thermal conductivity	4.0	$\text{W m}^{-1} \text{K}^{-1}$	[1]
κ	Thermal diffusivity	10^{-6}	$\text{m}^2 \text{s}^{-1}$	[1]
α	Thermal expansivity	2×10^{-6}	K^{-1}	[1]
g	Gravitational acceleration at surface	8.87	m s^{-2}	[3]
T_s	Surface temperature	730	K	[1]
R_p	Radius of Venus	6050	km	[3]
R_c	Core radius	3110	km	[4]
ρ_m	Mantle density	3551	kg m^{-3}	[1]
ρ_c	Core density	12,500	kg m^{-3}	[1]
P_{cm}	Pressure at core/mantle boundary	130	GPa	[1]
P_c	Pressure at the center of Venus	290	GPa	[1]
C_m	Specific heat of the mantle	1200	$\text{J kg}^{-1} \text{K}^{-1}$	[4]
C_c	Specific heat of the core	850	$\text{J kg}^{-1} \text{K}^{-1}$	[3]
η_m	Ratio of average and potential T for the mantle	1.3	–	[1]
η_c	Ratio of average and potential T for the core	1.2	–	[1]
L_m	Latent heat of mantle melting	6.0×10^5	J kg^{-1}	[5]
$(L_c + E_g)$	Heat release from inner core formation	5.0×10^5	J kg^{-1}	[5]
$(d\phi/dP)_S$	Melt productivity from adiabatic decompression	1.20×10^{-8}	Pa^{-1}	[6]
$(dT/dP)_S$	Adiabatic temperature gradient in the mantle	1.54×10^{-8}	K Pa^{-1}	[6]
<i>Variable</i>				
f	Fraction of core heat flux carried by plumes	–	–	–
E	Activation energy	–	kJ mol^{-1}	–
η_0	Reference viscosity	–	Pa s	–
ϕ	Melt fraction	–	–	–
V_{proc}/V_{SM}	Fraction of source mantle processed by melting	–	–	–
$M_{atm,^{40}\text{Ar}}$	Atmospheric mass of radiogenic argon	–	kg	–
$[K]_c$	Crustal abundance of potassium	–	wt.%	–
ΔT_{cm}	Temperature contrast across core/mantle boundary	–	K	–
$\Delta h_{c,0.5}$	Crustal production during the last 0.5 Gyr	–	km	–

and present-day values for the parameters illustrated in Fig. 2, as well as the present-day atmospheric mass of radiogenic argon and the modern crustal abundance of potassium.

5. Results

5.1. Sample thermal and chemical history

Simulations conform to observational constraints on the evolution of Venus for certain combinations of initial conditions. Fig. 3 shows the results of one representative example generated using $f = 0.25$, $E = 300 \text{ kJ mol}^{-1}$, $K/U = 7220$, $[U(t_p)]_{PM} = 17 \text{ ppb}$, $T_u(0) = 1900 \text{ K}$, $T_{cm}(0) = 4200 \text{ K}$, and $\log_{10}(\eta_0) = 20.5$. Core cooling is most intense as high temperatures from the “hot start” in the core are lost in the first ~ 1 Gyr. Since the mantle potential temperature actually increases for ~ 1.5 Gyr, core cooling quickly declines until ~ 2.2 Gyr. No inner core growth occurs within 4.5 Gyr, and the modern core only loses heat by conduction. That is, the total heat flux of 2.3 TW out of the core at present is probably insufficient to drive a dynamo by thermal convection alone (e.g., Pozzo et al., 2012; Gomi et al., 2013). This simulation satisfies the most basic criterion for the existence of mantle plumes: $F_{cm}(t_p) > 0 \text{ mW m}^{-2}$ (e.g., Weizman et al., 2001). The temperature contrast across the core/mantle boundary is $\Delta T_{cm}(t_p) \sim 60 \text{ K}$, roughly 40% less than the viscous temperature scale (Smrekar and Sotin, 2012). Plumes are still plausible in this simulation because our formulation of core heat flux assumes that the lower thermal boundary layer has already been thinned by the ejection of plumes, e.g., to a present-day $\sim 13 \text{ km}$ (Stevenson et al., 1983). Including radiogenic heating in the core or increasing the viscosity of the lower mantle would both tend to increase the core/mantle temperature contrast.

Crustal and lithosphere thicknesses calculated for the present are both within plausible ranges (e.g., Nimmo and McKenzie, 1998; James et al., 2013). The average crustal thickness calculated for the present is $\sim 30 \text{ km}$. This simulation also predicts an atmospheric mass of radiogenic argon within $0.14\text{--}\sigma$ of the measured, present-day value. The average crustal abundance of potassium is also near the mean value of existing measurements (e.g., Kaula, 1999). The initial spike visible in panel e occurs because ϕ is relatively large during the early epoch of rapid cooling. Mantle melting has cumulatively processed most of the source mantle, i.e., $V_{proc}(t_p) \approx 0.82 V_{SM}(t_p)$. Roughly 60% of the total inventory of heat-producing elements is sequestered in the crust at the end of the simulation. So, the volumetric heating of the source mantle at present is only $\sim 40\%$ of what would be produced in the undifferentiated primitive mantle. The normalized water concentration in the mantle is $C_{SM}^W \sim 0.45$ at the end of the simulation, meaning that the dehydration term in Eq. (11) is only $\sim 6\%$ of the other term inside the exponential. Thus, Venus can retain a significant portion of its initial interior inventory of volatiles for over 4.5 Gyr.

Rough estimates of the surface age of Venus are shown in panel f of Fig. 3. Because the one-dimensional model only returns a global average, we must calculate the time since a certain amount of crustal production occurred to estimate the fraction of the surface of Venus that has been resurfaced. For example, say a global average of 1 km of magmatism is required for complete resurfacing. Then, 50% of the surface would have an age of $\leq 1.5 \text{ Ga}$ if 0.5 km of crust were produced from 3 Gyr to the present, assuming that all magmatism is extrusive. To calculate estimated ages in Fig. 3, we assume that only 50% of crustal production causes resurfacing because some volcanism is likely intrusive. Thinner volcanic flows could cover a much larger fraction of the surface. In this simulation, an average of $\sim 132 \text{ m}$ of crust was produced during the last $\sim 500 \text{ Myr}$. Surface features like mountains or tall rims of large craters with ages $> 1.75 \text{ Ga}$ can remain unburied and thus visible in

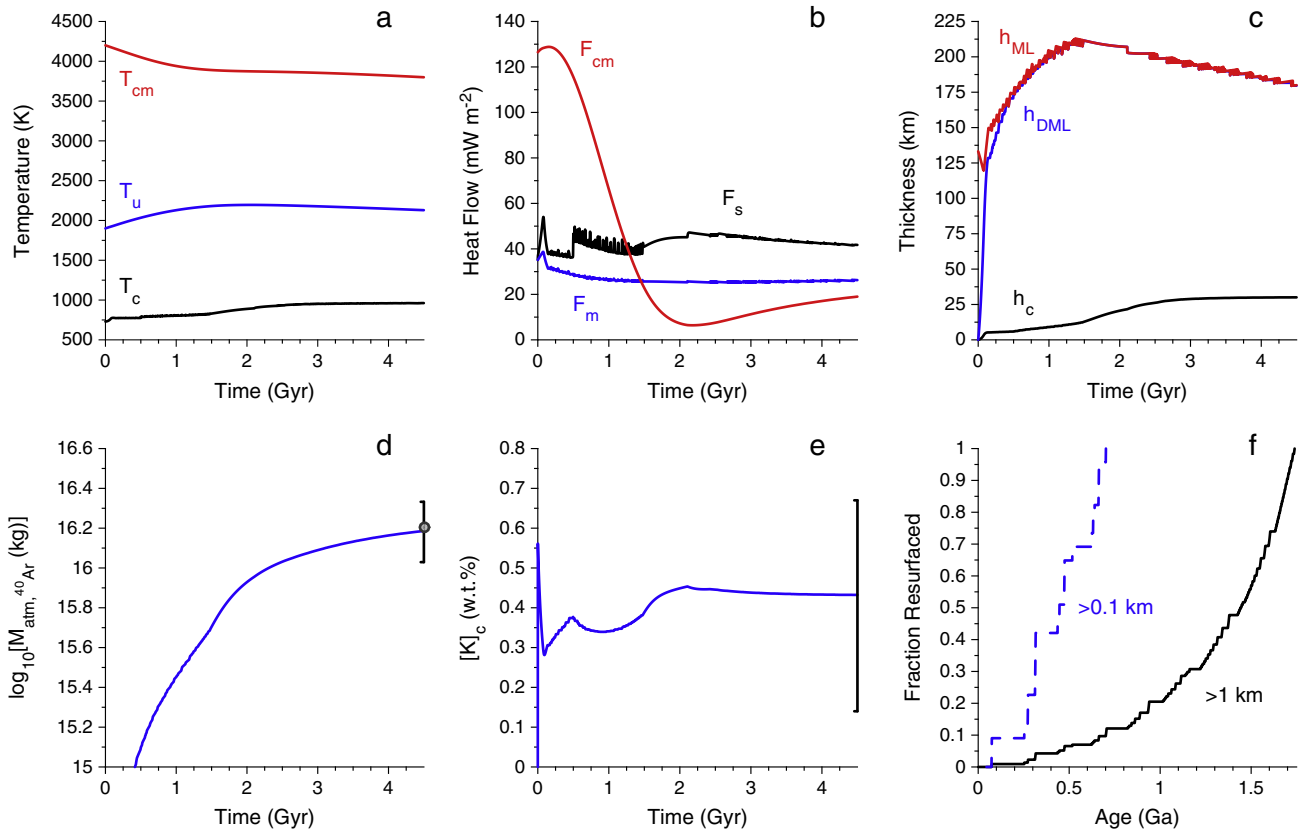


Fig. 3. Calculated thermal and chemical history for Venus with $f = 0.25$, $E = 300 \text{ kJ mol}^{-1}$, $K/U = 7220$, $[U(t_p)]_{PM} = 17 \text{ ppb}$, $T_u(0) = 1900 \text{ K}$, $T_{cm}(0) = 4200 \text{ K}$, and $\log_{10}(\eta_0) = 20.5$. (a) Core/mantle boundary, mantle potential, and Moho temperatures (red, blue, and black, respectively). (b) Core, mantle, and surface heat fluxes (red, blue, and black). The moving average of the surface heat flux is plotted with a 5 Myr span because basal melting of the crust may cause large discontinuities. (c) Crustal thickness (black), and thicknesses of the depleted mantle lithosphere (blue) and mantle lithosphere (red), which are nearly identical after $\sim 100 \text{ Myr}$. (d) Atmospheric mass of radiogenic argon (blue) and present-day measurement (point with $1-\sigma$ error bars). (e) Crustal abundance of potassium (blue) and range of plausible values from Venera and Vega landers (black vertical bar). (f) Cumulative fraction of Venus that has been resurfaced, on average, to a depth of at least 0.1 km (blue, dashed) and 1 km (black, solid) as a function of time before present, assuming that the amounts of intrusive and extrusive volcanism are equal. (For interpretation of the references to color in this figure legend, the reader is referred to the web version of this article.)

surface imagery. Studies of the cratering record likewise indicate that thin, post-impact flows have partially filled most craters, but much of the surface is possibly ancient nevertheless (e.g., Herrick and Rumpf, 2011; O'Rourke et al., 2014).

5.2. Sensitivity analyses

Fig. 4 shows the output of 1416 simulations of the evolution of Venus. Present-day values of important parameters are plotted against present-day crustal thickness. Because we conducted a grid search of a large parameter space, only 906 and 363 simulations produced the observed amount of radiogenic argon within 2- and 1- σ , respectively. Of the 363, 233 simulations also predict crustal production during the latest 500 Myr, of which 219 (red dots in Fig. 4) also have $F_{cm}(t_p) > 0 \text{ mW m}^{-2}$. The median and maximum core/mantle temperature contrasts are 63 K and 167 K, respectively, for simulations that satisfy the argon constraint within 1- σ and predict present-day core cooling. Simulations that have present-day crustal thicknesses up to 75 km can predict the observed amount of argon degassing within 1- σ . But all but three simulations with $h_c(t_p) > 50 \text{ km}$ fail to predict recent resurfacing and core cooling. Decreasing the assumed efficiency of argon degassing on Venus could proportionally increase this limit on the amount of crustal production that can occur throughout geologic time.

To further examine the first-order correlations between the simulation results, we calculate the first principal component basis vector, which is the axis representing the majority (52.67%) of the variance in the output dataset (e.g., O'Rourke and Korenaga, 2012). Coefficients in the basis vector, listed under Π_1 in Table 2, could range from -1 to 1 in principle. Large absolute values indicate coefficients that are important to explaining the variance in the dataset. If two parameters have opposite or identical signs, then they are anticorrelated or correlated, respectively. Arrows representing projections of the basis vector are also plotted in Fig. 4. Basis vectors have no preferred polarity, so the signs of the values and directions of the arrows could all be reversed with no loss of information.

Crustal production is the dominant factor controlling variance in the simulation results. Three of the largest coefficients in the basis vector are associated with T_c (0.32), h_c (0.31), and V_{proc}/V_{SM} (0.30). Visual inspection of Fig. 4 confirms that thick crust is typically hot, and producing thick crust requires a high degree of mantle processing. Other correlations between parameters in the basis vector have physical explanations. The thicknesses of both the ML and the DML are strongly anticorrelated with crustal thickness (coefficients of -0.33 and -0.32) because the relatively hot mantle that produces thick crust tends to destabilize the DML. Increasing $V_{proc}(t_p)$ promotes additional ^{40}Ar degassing and a larger absolute mass of K tends to partition into the crust, although $[K(t_p)]_c$ may actually decrease as crustal volume increases. Note that the mantle

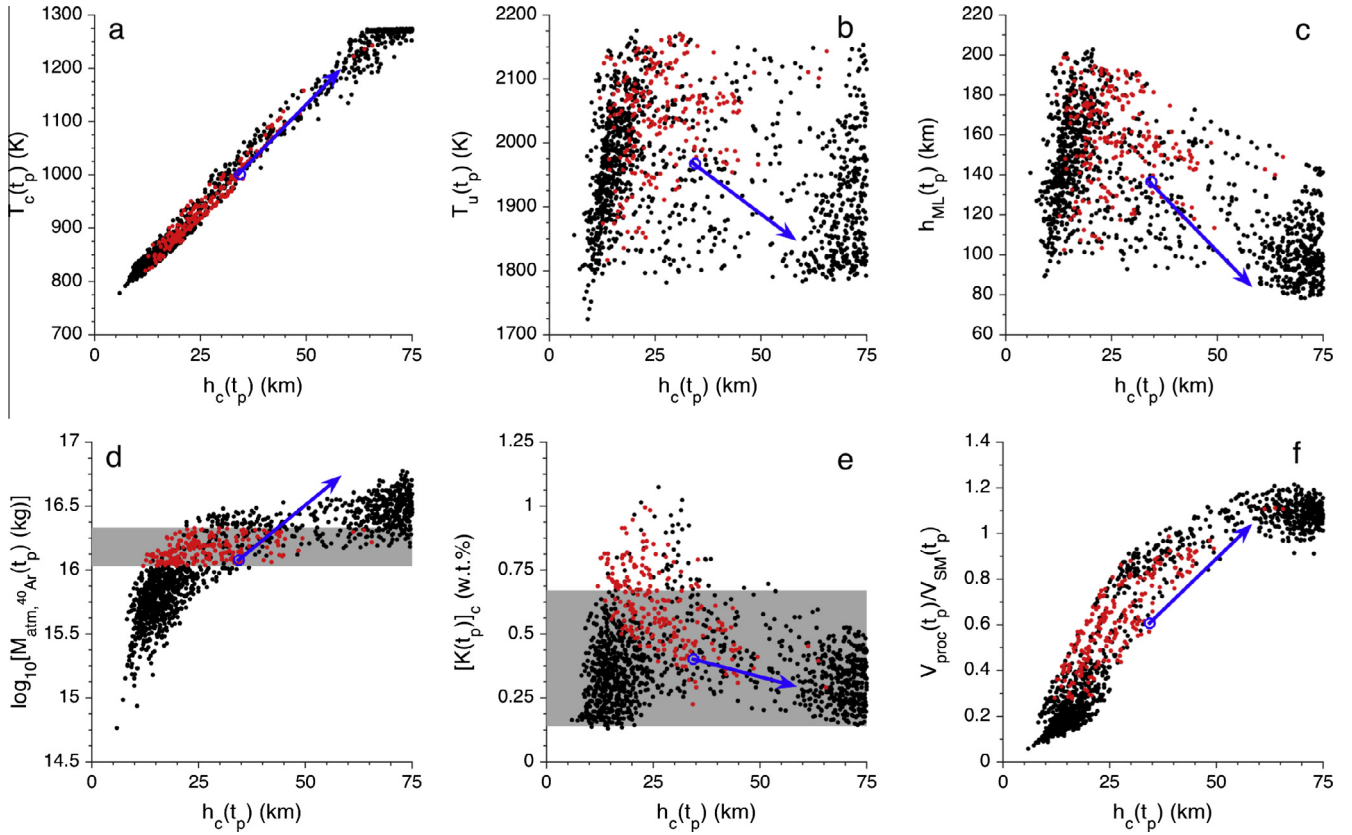


Fig. 4. Summary of the results of 1416 simulations of the thermal and chemical evolution of Venus. Panels compare current crustal thickness to present-day values of (a) Moho temperature, (b) mantle potential temperature, (c) mantle lithosphere thickness, (d) atmospheric mass of radiogenic argon, (e) crustal abundance of potassium, and (f) fraction of the source mantle that has been processed by partial melting. The blue arrows are projections of the first principal component basis vector emanating from points representing the averaged simulation results. This vector indicates the axis accounting for the majority of the variance in the dataset, as explained in the text. The present-day atmospheric mass of radiogenic argon (1- σ interval) and the range of measured crustal abundances of potassium are shown as shaded gray regions in (d) and (e), respectively. Red dots indicate the 219 simulations that satisfy the argon constraint and feature crustal production during the latest 500 Myr and present-day core cooling. (For interpretation of the references to color in this figure legend, the reader is referred to the web version of this article.)

Table 2
First principal component basis vector (Π_1) and coefficients for the best-fit linear function relating present-day parameter values ($C_{i,0}$ through $C_{i,6}$). Correlation coefficients quantifying the correspondence between the actual and predicted output parameters are also included. To calculate the best-fit function, the input parameters were first mean-subtracted using their average values: $E = 346.36 \text{ kJ mol}^{-1}$, $K/U = 10,024$, $[U(t_p)]_{PM} = 16.10 \text{ ppb}$, $T_u(0) = 1623.66 \text{ K}$, $T_{cm}(0) = 4152.26 \text{ K}$, and $\log_{10}(\eta_0) = 19.89$. They were then normalized by $40.68 \text{ kJ mol}^{-1}$, 2640 , 2.66 ppb , 116.13 K , 155.44 K , and 0.55 , respectively.

P_i	Π_1	$C_{i,0}$	$C_{i,1}$	$C_{i,2}$	$C_{i,3}$	$C_{i,4}$	$C_{i,5}$	$C_{i,6}$	Units	Corr.
$T_c(t_p)$	0.32	1001.24	99.46	78.73	-112.60	103.61	57.51	35.34	K	0.84
$T_u(t_p)$	-0.23	1967.78	20.63	18.96	75.58	31.66	16.18	-18.70	K	0.94
$T_{cm}(t_p)$	-0.18	3567.54	42.13	41.24	83.28	43.72	23.98	-21.95	K	0.98
$h_c(t_p)$	0.31	34.38	13.73	10.56	-14.21	13.86	7.80	4.66	km	0.84
$h_{DML}(t_p)$	-0.33	132.79	-2.83	-3.04	29.27	-1.49	-1.14	-7.99	km	0.87
$h_{ML}(t_p)$	-0.32	136.45	-1.33	-2.85	26.05	-1.18	-0.84	-6.01	km	0.85
$F_s(t_p)$	0.29	41.11	1.86	1.17	-3.58	3.73	1.62	0.98	mW m^{-2}	0.83
$F_m(t_p)$	-0.06	28.99	-1.97	-1.05	-0.13	-1.72	-0.98	-0.40	mW m^{-2}	0.81
$V_{proc}(t_p)/V_{SM}(t_p)$	0.30	0.61	0.27	0.15	-0.24	0.26	0.14	0.09	-	0.90
$M_{atm,40Ar}(t_p)$	0.26	16.08	0.25	0.11	-0.22	0.25	0.22	0.08	$\log_{10}(\text{kg})$	0.98
$[K(t_p)]_c$	-0.08	0.40	0.01	-0.04	0.02	0.06	0.10	0.00	wt.%	0.73

still retains volatiles with $V_{proc} > V_{SM}$ because it is assumed to homogenize between each episode of melting.

A linear function of initial conditions provides a quick, simple way to roughly estimate present-day model parameters (e.g., O'Rourke and Korenaga, 2012). The general formula is

$$P_i(t_p) = C_{i,0} + C_{i,1}T_{u,n}(0) + C_{i,2}T_{cm,n}(0) + C_{i,3}[\log_{10}(\eta_0)]_n + C_{i,4}[U(t_p)]_{PM,n} + C_{i,5}(K/U)_n + C_{i,6}E_n, \quad (36)$$

where P_i is the present-day value of the i th output parameter; constants $C_{i,0}$ through $C_{i,6}$ are calculated using the least squares method for each P_i ; and each subscript n indicates that the input parameters are mean-subtracted and normalized by their standard deviations, while the output parameters remain dimensional. Table 2 contains the calculated best-fit coefficients and the correlation coefficients between predicted values and model output, where numbers close to 1 indicate a good fit. The utilized values for the average and standard deviation of the input parameters are also listed.

Values of $C_{i,1}$ through $C_{i,6}$ indicate which initial conditions are most important to the simulation results. For instance, η_0 mostly controls how hot the mantle is at present, along with $[U]_{PM}$. Crustal thickness, in contrast, depends slightly more on the initial temperatures of the core and mantle, since most crustal production occurs in early epochs. Since the mantle insulates the core, the temperature of the core today depends largely on the initial interior temperatures and η_0 , which govern how quickly the mantle loses heat. Increasing E tends to produce the opposite effects as increasing the reference viscosity. That is, high values of E are associated with more mantle melting, thin lithosphere, thick crust, and a cold mantle and core. High values of E correspond to low values of the preexponential constant, A , in our parameterization of viscosity (Eq. (11)). Therefore, absolute viscosity is actually decreased for increased values of E at typical mantle potential temperatures above the reference temperature. If A were held constant, then decreasing E would produce lower absolute viscosity and thus more vigorous convection. In any case, varying η_0 by only an order of magnitude is equivalent to a large ($\sim 250 \text{ kJ mol}^{-1}$) change in E , so our simulations are not very sensitive to the uncertainty in this parameter.

Although many combinations of initial conditions produce too much or too little degassing, all values of individual initial conditions are represented in the suite of simulations with the correct amount of argon degassing and recent volcanism. Any choice of $[U(t_p)]_{PM}$, for example, is permissible if other parameters are suitably adjusted. Each initial condition except E is of roughly equal importance. Increased mantle viscosity inhibits argon degassing by decreasing convective velocities and thus melt production. High internal temperatures and radiogenic heating promote argon degassing, so Venus cannot have extreme values of all these initial conditions unless some of our fundamental assumptions about planetary evolution are incorrect.

The predictive power of the best-fit linear functions for most model parameters is quite good. Correlation coefficients for present-day values of F_s , F_m , h_{DML} , and h_{ML} are high even though they can exhibit variability over short time intervals during simulations. The best-fit function tends to fail near extreme values of some parameters. For example, while crustal thickness is well predicted in general, the best-fit function underestimates crustal thickness for $h_c < 10 \text{ km}$ by predicting unphysical, negative values. Likewise, the best-fit function for Moho temperature returns poor predictions for the coldest and hottest temperatures. As seen in Fig. 4, basal melting in the crust causes non-linearity for high Moho temperatures, whereas the large number of simulations with extremely cold initial conditions harms the fit for Moho temperatures close to the surface temperature. Linear functions for key model results can be used to quickly guess whether a given set of initial conditions will yield present-day parameters consistent with observational constraints. However, thermal evolution simulations are still required to confirm these approximate predictions.

The simulation shown in Fig. 3 was repeated 50 times with f varied between the extreme values of 0.01 and 0.5. For the nominal value of $f = 0.25$, $\Delta h_{c,0.5} = 132 \text{ m}$ is the globally averaged increase in crustal thickness during the last 0.5 Gyr. This value remains essentially unchanged as f is decreased to 0.01. However, setting $f = 0.4$ – 0.5 increases the heat flux from mantle plumes during the early evolution of Venus, causing efficient cooling of the mantle and limiting the recent increase in crustal thickness to $\Delta h_{c,0.5} \approx 70 \text{ m}$. However, high melt fractions during early evolution cause the total crustal production to increase by ~ 5 – 10 km . In contrast, $h_c(t_p) = 22 \text{ km}$ when $f = 0.01$, a decrease of 8 km from the nominal result. The total amount of argon degassing is less sensitive to changes in f , varying by $\sim 12\%$ (or $0.35\text{-}\sigma$) over the entire range of values. Mantle plumes that upwell relatively late in the evolution

of Venus have little effect on the present-day atmospheric abundance of radiogenic argon because most mantle processing and sequestration of ^{40}K in the crust occurs early.

6. Discussion

6.1. Thermal evolution of Venus

Stagnant-lid convection is perhaps the expected regime of mantle dynamics for Venus. Introducing plate tectonics or additional mechanisms for surface recycling requires substantial justification, especially because the initialization of plate tectonics on Earth largely remains a mystery (e.g., Korenaga, 2013). Deviations from the stagnant-lid regime have been incorporated into models of the evolution of Venus to explain a putative global resurfacing event at $\sim 500 \text{ Ma}$. However, if the requirement for a rapid, global resurfacing event is rejected in favor of more gradual resurfacing (e.g., Guest and Stofan, 1999; Hansen and Lopez, 2010; O'Rourke et al., 2014), a model of stagnant-lid convection can reproduce significant features of present-day Venus to first order. In particular, both decompression melting of passively upwelling mantle and volcanism from mantle plumes can explain the young-looking surface of Venus. Melting of passive upwellings is relatively more important to recent crustal production and argon degassing, but mantle plumes may have important effects on local geology.

Thermal evolution models that satisfy the argon constraint are non-unique (e.g., O'Neill et al., 2014), just as the observed geological features and cratering statistics admit a range of possible evolutionary scenarios. For example, a single episode of mantle melting during a catastrophic resurfacing event releases the requisite mass of radiogenic argon for crustal thicknesses of ~ 10 – 50 km , within the estimated present-day range (e.g., James et al., 2013). Unlike simulations of stagnant-lid convection, the suitability of this simple model is not sensitive to the uncertainties in the chemical composition of Venus. Of course, a history with only one melting event is both extremely simplistic and highly unlikely, but it serves to demonstrate the important caveat that argon degassing alone does not unambiguously point towards a single path for the thermal evolution of Venus.

Many important issues await further study. We calculated approximate surface ages based on the global average of crustal thickness, but the fraction of melt production that causes resurfacing is uncertain. That is, the ratio of extrusive to intrusive volcanism depends on the poorly known density difference between melt and solid phases in the crust and lithosphere of Venus, which is probably a complicated function of composition and depth (e.g., Crisp, 1984; White et al., 2006; Reese et al., 2007). A higher fraction of intrusive magmatism mandates a larger amount of recent melt production to explain the young-looking surface of Venus. The total crustal production cannot exceed $\sim 65 \text{ km}$, however, without violating the argon constraint unless argon is actually compatible in basaltic magma and/or diffusion is slow (e.g., Watson et al., 2007). Intriguingly, Watson et al. (2007) invoked hydration of oceanic lithosphere to release ^{40}Ar into Earth's atmosphere, which seems to imply that ^{40}Ar in the atmosphere of Venus is evidence that stable, water oceans existed in the past. On the other hand, the interpretation of their data is controversial, and the behavior of ^{40}Ar might actually match conventional assumptions (e.g., Namiki and Solomon, 1998; Kaula, 1999; Cassata et al., 2011).

Our simulations generally predict that the core continuously cools. The calculated temperature differences across the core/mantle boundary are typically near the values considered sufficient to drive plume formation (Smrekar and Sotin, 2012). Models of the

evolution of the core could include additional complications to possibly better match observational evidence for mantle plumes. Our simulations do not include heat-producing elements like potassium or uranium in the core, although experimental evidence typically favors <80 ppm of potassium in Earth's core, corresponding to <0.5 TW of radiogenic heating (e.g., [Corgne et al., 2007](#)). More generally, we assume that the entire core is homogenous and convective. Future studies must also consider the possibly high thermal conductivity and compositional stratification that may develop during accretion (e.g., [Pozzo et al., 2012](#); [Rubie et al., 2015](#)). Unfortunately, the structure and composition of the core of Venus is essentially unconstrained. Introducing these additional complications will only increase the flexibility of our models, reinforcing our conclusion that continuous evolution in the stagnant-lid regime is consistent with available observations.

6.2. Comparison with other studies

Any one-dimensional, parameterized model suffers some shortcomings. We cannot address the relationship between gravity and topography on Venus, which is an important constraint on higher-dimensional models (e.g., [Armann and Tackley, 2012](#)). More importantly, our fundamental assumption is that scaling laws developed for steady-state convection yield reasonably good approximations for the properties of the convective system at each time step. When crustal formation occurs, for example, the associated loss of potassium and argon is assumed to instantly decrease their respective abundances in the entire convecting mantle. This approach has been validated for simple systems with uniform viscosity or purely temperature-dependent viscosity (e.g., [Daly, 1980](#); [Choblet and Sotin, 2000](#)). But steady-state models are probably ill-suited to capturing transient events that likely occurred during the early evolution of Venus, like the crystallization of a magma ocean (e.g., [Solomatov and Stevenson, 1993](#)) and large impacts (e.g., [Agnor et al., 1999](#)). Furthermore, our models do not accommodate transitions in convective regimes or differences in rheology, composition, or hydration between an upper and lower mantle (e.g., [Papuc and Davies, 2012](#); [Ogawa and Yanagisawa, 2014](#)).

[Armann and Tackley \(2012\)](#) argued that continuous evolution in the stagnant-lid regime tends to produce an unrealistically high rate of recent resurfacing. Our methods and conclusions differ in several respects. Their choice of radiogenic heating in the mantle corresponds to the canonical $[U(t_p)]_{PM} = 21$ ppb and $K/U = 7220$, whereas we consider a wider range of possible values consistent with uncertainties on the composition of bulk silicate Earth ([Lyubetskaya and Korenaga, 2007](#)). Moreover, [Armann and Tackley \(2012\)](#) include geochemically dubious concentrations of potassium in the core: 400–800 ppm, which produce ~ 3 –6 TW of extra heating. Crustal recycling in their models prevents all heat-producing elements from partitioning into the crust, despite a relatively large amount of mantle processing. We do not include crustal recycling here, which is partially justified because crust thick enough to transition to eclogite and sink into the mantle tends to violate the argon constraint under the assumption of efficient degassing. Ultimately, we agree that roughly half of the total inventory of heat-producing elements is plausibly sequestered in the crust of Venus. We also confirm that higher mantle viscosity should reduce the total amount of melt production, although their low-viscosity case has efficient recycling and thus produces thinner crust at present. Of course, we do not use the low values for yield stress that [Armann and Tackley \(2012\)](#) introduced to produce catastrophic resurfacing events.

Our different treatments of mantle melting are also responsible for our divergent results. [Armann and Tackley \(2012\)](#) predict that

melt migration is the primary mode of heat transport, whereas our results suggest that conduction through the upper thermal boundary layer is relatively more important. In our models, partial melting of the mantle forms a depleted layer in the lithosphere that impedes further magmatism. [Armann and Tackley \(2012\)](#) make an “end-member assumption” that any melt produced in a zone with depth up to 600 km is instantaneously extruded onto the surface, justified by the likely fact that buoyant melt moves faster than the average convective velocity. Depleted material is thus left behind and may be efficiently recycled deep in the convecting mantle. Consequently, their models produce relatively more melt. Future studies are needed to determine the extent to which reality resembles these two approximations.

Parameterized models ultimately complement direct simulations of planetary evolution that include additional complications. Direct simulations are often sensitive to values of parameters that are poorly constrained by observations, such as reference viscosity, melt transport, and density differences between various mantle phases (e.g., [Armann and Tackley, 2012](#); [Ogawa and Yanagisawa, 2014](#)). The computational expense of running a complete sensitivity analysis on direct simulations is potentially prohibitive. So, parameterized models remain valuable because they are relatively straightforward to understand and the effects of various assumptions are easily explored. If direct simulations systematically disagree with predictions from parameterized models, then perhaps new theoretical scalings can be developed that will both help models match observations and increase our understanding of the underlying processes.

7. Conclusions

Multiple scenarios for the evolution of Venus may satisfy constraints imposed by surface geology and the present-day atmospheric mass of radiogenic argon. Periodic episodes of global resurfacing are a popular explanation for the young-looking surface of Venus. Indeed, a catastrophic resurfacing event at ~ 500 Ma would produce a crustal thickness and magnitude of argon degassing that match current estimates, even considering the large uncertainties on the chemical composition of Venus. Drastic departures from the stagnant-lid regime of mantle convection, however, would be required to produce short-duration global resurfacing events. Many mechanisms have been proposed, but continuous evolution with a stagnant lid remains the simplest scenario and the default regime of mantle convection, according to theory. Moreover, impact crater statistics and recent geologic mapping are also consistent with resurfacing from localized, non-catastrophic volcanism.

Self-consistent thermal evolution models of stagnant-lid convection can predict the correct amount of argon degassing. Because many important parameters are poorly constrained, sensitivity analyses are critical to determine the relationships between initial conditions and modeling results. Principal component analysis was used to identify the largest source of variations in the simulation output. A linear function of input parameters can predict many parameters of interest to reasonable accuracy. This provides a shortcut to finding the space of initial conditions that will produce, for example, acceptable amounts of argon degassing and crustal and lithosphere thicknesses that match geophysical models. Furthermore, the coefficients in the best-fit function help identify the initial conditions with the strongest control over simulation results. Simulations that satisfy the argon constraint also predict limited core cooling, which prevents dynamo action today but also causes mantle plume upwellings, providing a source of recent volcanism and an explanation for observed surface features on Venus.

Acknowledgments

This material is based upon work supported by the National Science Foundation Graduate Research Fellowship under Grant No. DGE-1144469. J.G. O'Rourke thanks CT Space Grant and the George J. Schultz Fellowship from Yale University's Silliman College for past support. Two anonymous reviewers provided comments that considerably improved the content and clarity of this paper.

References

- Agnor, C.B., Canup, R.M., Levison, H.F., 1999. On the character and consequences of large impacts in the late stage of terrestrial planet formation. *Icarus* 142, 219–237.
- Arevalo, R., McDonough, W.F., Luong, M., 2009. The K/U ratio of the silicate Earth: Insights into mantle composition, structure and thermal evolution. *Earth Planet. Sci. Lett.* 278, 361–369.
- Armann, M., Tackley, P.J., 2012. Simulating the thermochemical magmatic and tectonic evolution of Venus's mantle and lithosphere: Two-dimensional models. *J. Geophys. Res.* 117, E12003.
- Bills, B.G., Jones, R.L., Kiefer, W.S., 1987. Venus gravity: A harmonic analysis. *J. Geophys. Res.* 92, 10335–10351.
- Bjornnes, E. et al., 2012. Equilibrium resurfacing of Venus: Results from new Monte Carlo modeling and implications for Venus surface histories. *Icarus* 217, 451–461.
- Bullock, M., Grinspoon, D.H., 2001. The recent evolution of climate on Venus. *Icarus* 150, 19–37.
- Cassata, W.S., Renne, P.R., Shuster, D.L., 2011. Argon diffusion in pyroxenes: Implications for thermochronometry and mantle degassing. *Earth Planet. Sci. Lett.* 304, 407–416.
- Choblet, G., Sotin, C., 2000. 3D thermal convection with variable viscosity: Can transient cooling be described by a quasi-static scaling law? *Phys. Earth Planet. Inter.* 119, 321–336.
- Corgne, A. et al., 2007. How much potassium is in the Earth's core? New insights from partitioning experiments. *Earth Planet. Sci. Lett.* 256, 567–576.
- Crisp, J.A., 1984. Rates of magma emplacement and volcanic output. *J. Volcanol. Geoth. Res.* 20, 177–211.
- Daly, S.F., 1980. Convection with decaying heat sources: constant viscosity. *Geophys. J. Int.* 61, 519–547.
- Driscoll, P., Bercovici, D., 2013. Divergent evolution of Earth and Venus: Influence of degassing, tectonics, and magnetic fields. *Icarus* 226, 1447–1464.
- Driscoll, P., Bercovici, D., 2014. On the thermal and magnetic histories of Earth and Venus: Influences of melting, radioactivity, and conductivity. *Phys. Earth Planet. Inter.* 236, 36–51.
- Fegley, B., Prinn, R., 1989. Estimation of the rate of volcanism on Venus from reaction rate measurements. *Nature* 337, 55–58.
- Fowler, A., O'Brien, S., 1996. A mechanism for episodic subduction on Venus. *J. Geophys. Res.* 101, 4755–4763.
- Fraeman, A.A., Korenaga, J., 2010. The influence of mantle melting on the evolution of Mars. *Icarus* 210, 43–57.
- Gillmann, C., Tackley, P., 2014. Atmosphere/mantle coupling and feedbacks on Venus. *J. Geophys. Res.: Planets* 119, 1189–1217.
- Gomi, H. et al., 2013. The high conductivity of iron and thermal evolution of the Earth's core. *Phys. Earth Planet. Inter.* 224, 88–103.
- Guest, J., Stofan, E.R., 1999. A new view of the stratigraphic history of Venus. *Icarus* 139, 55–66.
- Hansen, V., Lopez, I., 2010. Venus records a rich early history. *Geology* 38, 311–314.
- Hauck, S.A., Phillips, R.J., 2002. Thermal and crustal evolution of Mars. *J. Geophys. Res.* 107, 1–19.
- Herrick, R.R., Rumpf, M.E., 2011. Postimpact modification by volcanic or tectonic processes as the rule, not the exception, for Venusian craters. *J. Geophys. Res.* 116, E02004.
- Herrick, R.R., Sharpton, V.L., 2000. Implications from stereo-derived topography of Venusian impact craters. *J. Geophys. Res.* 105, 20245.
- Ivanov, M.A., Head, J.W., 2013. The history of volcanism on Venus. *Planet. Space Sci.* 84, 66–92.
- James, P.B., Zuber, M.T., Phillips, R.J., 2013. Crustal thickness and support of topography on Venus. *J. Geophys. Res. E: Planets* 118, 859–875.
- Karato, S., Wu, P., 1993. Rheology of the upper mantle: A synthesis. *Science* 260, 771–778.
- Kaula, W., 1999. Constraints on Venus evolution from radiogenic argon. *Icarus* 139, 32–39.
- Kaula, W., Phillips, R., 1981. Quantitative tests for plate tectonics on Venus. *Geophys. Res. Lett.* 8, 1187–1190.
- Korenaga, J., 2002. Methods for resolving the origin of large igneous provinces from crustal seismology. *J. Geophys. Res.*, 107
- Korenaga, J., 2006. Archean geodynamics and the thermal evolution of Earth. *Archean Geodynamics Environ.* 164, 7–32.
- Korenaga, J., 2007. Thermal cracking and the deep hydration of oceanic lithosphere: A key to the generation of plate tectonics? *J. Geophys. Res.* 112, 1–20.
- Korenaga, J., 2009. Scaling of stagnant-lid convection with Arrhenius rheology and the effects of mantle melting. *Geophys. J. Int.* 179, 154–170.
- Korenaga, J., 2013. Initiation and evolution of plate tectonics on Earth: Theories and observations. *Annu. Rev. Earth Planet. Sci.* 41, 117–151.
- Landuyt, W., Bercovici, D., 2009. Variations in planetary convection via the effect of climate on damage. *Earth Planet. Sci. Lett.* 277, 29–37.
- Lenardic, A., Jellinek, A., Moresi, L.N., 2008. A climate induced transition in the tectonic style of a terrestrial planet. *Earth Planet. Sci. Lett.* 271, 34–42.
- Leng, W., Zhong, S., 2008. Controls on plume heat flux and plume excess temperature. *J. Geophys. Res.: Solid Earth* 113, 1–15.
- Lyubetskaya, T., Korenaga, J., 2007. Chemical composition of Earth's primitive mantle and its variance: 1. Method and results. *J. Geophys. Res.* 112, B03211.
- McDonough, W., Sun, S., 1995. The composition of the Earth. *Chem. Geol.* 120, 223–253.
- McKinnon, W.B. et al., 1997. Cratering on Venus: Models and observations. In: *Venus II. Arizona Univ. Press*, pp. 969–1014.
- Moresi, L.M., Solomatov, V., 1998. Mantle convection with a brittle lithosphere: Thoughts on the global tectonic styles of the Earth and Venus. *Geophys. J. Int.* 133, 669–682.
- Namiki, N., Solomon, S., 1993. The gabbro-eclogite phase transition and the elevation of mountain belts on Venus. *J. Geophys. Res.* 98, 25–31.
- Namiki, N., Solomon, S.C., 1998. Volcanic degassing of argon and helium and the history of crustal production on Venus. *J. Geophys. Res.* 103, 3655.
- Nimmo, F., McKenzie, D., 1998. Volcanism and tectonics on Venus. *Annu. Rev. Earth Planet. Sci.* 26, 23–51.
- Nimmo, F., Stevenson, D.J., 2001. Estimates of martian crustal thickness from viscous relaxation of topography. *J. Geophys. Res.* 106, 5085–5098.
- Noack, L., Breuer, D., Spohn, T., 2012. Coupling the atmosphere with interior dynamics: Implications for the resurfacing of Venus. *Icarus* 217, 484–498.
- Ogawa, M., Yanagisawa, T., 2014. Mantle evolution in Venus due to magmatism and phase transitions: From punctuated layered convection to whole-mantle convection. *J. Geophys. Res.: Planets* 119, 867–883.
- O'Neill, C. et al., 2014. Mantle convection and outgassing on terrestrial planets. In: *Comparative Climatology of Terrestrial Planets*. Univ. of Arizona Press, Tucson, pp. 473–486.
- O'Rourke, J.G., Korenaga, J., 2012. Terrestrial planet evolution in the stagnant-lid regime: Size effects and the formation of self-destabilizing crust. *Icarus* 221, 1043–1060.
- O'Rourke, J.G., Wolf, A.S., Ehlmann, B.L., 2014. Venus: Interpreting the spatial distribution of volcanically modified craters. *Geophys. Res. Lett.* 41, 8252–8260.
- Orth, C.P., Solomatov, V.S., 2011. The isostatic stagnant lid approximation and global variations in the Venusian lithospheric thickness. *Geochem. Geophys. Geosyst.* 12, 1–17.
- Papuc, A.M., Davies, G.F., 2012. Transient mantle layering and the episodic behaviour of Venus due to the 'basalt barrier' mechanism. *Icarus* 217, 499–509.
- Phillips, R.J., Hansen, V.L., 1998. Geological evolution of Venus: Rises, plains, plumes, and plateaus. *Science* 279, 1492–1497.
- Phillips, J.L., Russell, C.T., 1987. Revised upper limit on the internal magnetic moment of Venus. *J. Geophys. Res.* 92, 2253–2263.
- Phillips, R.J., Bullock, M.A., Hauck, S.A., 2001. Climate and interior coupled evolution on Venus. *Geophys. Res. Lett.* 28, 1779–1782.
- Phillips, R.J. et al., 1992. Impact craters and Venus resurfacing history. *J. Geophys. Res.* 97, 15923.
- Pozzo, M. et al., 2012. Thermal and electrical conductivity of iron at Earth's core conditions. *Nature* 485, 355–358.
- Reese, C., Solomatov, V., Moresi, L., 1999. Non-newtonian stagnant lid convection and magmatic resurfacing on Venus. *Icarus* 80, 67–80.
- Reese, C.C., Solomatov, V.S., Orth, C.P., 2007. Mechanisms for cessation of magmatic resurfacing on Venus. *J. Geophys. Res.* 112, 1–12.
- Rubie, D. et al., 2015. Accretion and differentiation of the terrestrial planets with implications for the compositions of early-formed Solar System bodies and accretion of water. *Icarus* 248, 89–108.
- Schaber, G.G. et al., 1992. Geology and distribution of impact craters on Venus: What are they telling us? *J. Geophys. Res.* 97, 13257.
- Schubert, G., 1994. Gravity over coronae and chasmata on Venus. *Icarus* 112, 130–146.
- Schubert, G., Turcotte, D.L., Olson, P., 2001. *Mantle Convection in the Earth and Planets*. Cambridge University Press, New York.
- Shaw, D.M., 1970. Trace element fractionation during anatexis. *Geochim. Cosmochim. Acta* 34, 237–243.
- Simons, M., Solomon, S.C., Hager, B.H., 1997. Localization of gravity and topography: Constraints on the tectonics and mantle dynamics of Venus. *Geophys. J. Int.* 131, 24–44.
- Sleep, N.H., 1979. Thermal history and degassing of the Earth: Some simple calculations. *J. Geol.* 87, 671–686.
- Smrekar, S.E., 1994. Evidence for active hotspots on Venus from analysis of Magellan gravity data. *Icarus* 112, 2–26.
- Smrekar, S.E., Sotin, C., 2012. Constraints on mantle plumes on Venus: Implications for volatile history. *Icarus* 217, 510–523.
- Smrekar, S.E. et al., 2010. Recent hotspot volcanism on Venus from VIRTIS emissivity data. *Science* 328, 605–608.
- Solomatov, V.S., 1995. Scaling of temperature- and stress-dependent viscosity convection. *Phys. Fluids* 7, 266.
- Solomatov, V.S., Moresi, L.N., 1996. Stagnant lid convection on Venus. *J. Geophys. Res.* 101, 4737–4753.

- Solomatov, V.S., Moresi, L.N., 2000. Scaling of time-dependent stagnant lid convection: Application to small-scale convection on Earth and other terrestrial planets. *J. Geophys. Res.* 105, 21795–21817.
- Solomatov, V.S., Stevenson, D.J., 1993. Nonfractional crystallization of a terrestrial magma ocean. *J. Geophys. Res.* 98, 5391–5406.
- Spohn, T., 1991. Mantle differentiation and thermal evolution of Mars, Mercury, and Venus. *Icarus* 236, 222–236.
- Stevenson, D.J., 2003. Planetary magnetic fields. *Earth Planet. Sci. Lett.* 208, 1–11.
- Stevenson, D.J., Spohn, T., Schubert, G., 1983. Magnetism and thermal evolution of the terrestrial planets. *Icarus* 489, 466–489.
- Stofan, E.R. et al., 1995. Large topographic rises on Venus: Implications for mantle upwelling. *J. Geophys. Res.* 100, 317–327.
- Strom, R., Schaber, G., Dawson, D., 1994. The global resurfacing of Venus. *J. Geophys. Res.* 99, 10899–10926.
- Tajika, E., Matsui, T., 1993. Evolution of seafloor spreading rate based on 40-Ar degassing history. *Geophys. Res. Lett.* 20, 851–854.
- Tarduno, J.A. et al., 2010. Geodynamo, solar wind, and magnetopause 3.4 to 3.45 billion years ago. *Science* 327, 1238–1240.
- Treiman, A.H., 2007. Geochemistry of Venus' surface: Current limitations as future opportunities. In: Esposito, L.W., Stofan, E.R., Cravens, T.E. (Eds.), *Exploring Venus as a Terrestrial Planet*. American Geophysical Union, Washington, DC, pp. 7–22.
- Turcotte, D.L., 1993. An episodic hypothesis for Venusian tectonics. *J. Geophys. Res.* 98, 17061–17068.
- Watson, E.B., Thomas, J.B., Cherniak, D.J., 2007. ⁴⁰Ar retention in the terrestrial planets. *Nature* 449, 299–304.
- Weizman, A. et al., 2001. Modeling the volcanism on Mars. *Icarus* 150, 195–205.
- White, S.M., Crisp, J.A., Spera, F.J., 2006. Long-term volumetric eruption rates and magma budgets. *Geochem. Geophys. Geosyst.* 7, Q03010.
- Wichman, R.W., 1999. Internal crater modification on Venus: Recognizing crater-centered volcanism by changes in floor morphometry and floor brightness. *J. Geophys. Res.* 104, 21957–21977.
- Xie, S., Tackley, P.J., 2004. Evolution of helium and argon isotopes in a convecting mantle. *Phys. Earth Planet. Inter.* 146, 417–439.
- Yamazaki, D., Karato, S.i., 2001. Some mineral physics constraints on the rheology and geothermal structure of Earth's lower mantle. *Am. Mineral.* 86, 385–391.
- von Zahn, U. et al., 1983. Composition of the Venus atmosphere. In: Hunten, D.M., Colin, L., Donahue, T.M., Moroz, V.I. (Eds.), *Venus*. Univ. of Arizona Press, Tucson, pp. 299–430.
- Zhang, P., Cohen, R.E., Haule, K., 2015. Effects of electron correlations on transport properties of iron at Earth's core conditions. *Nature* 517, 605–607.